International Journal of Applied Earth Observations and Geoinformation 112 (2022) 102899

Contents lists available at ScienceDirect

International Journal of Applied Earth Observations and Geoinformation

journal homepage: www.elsevier.com/locate/jag

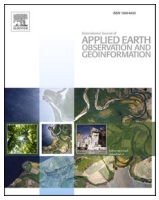

Operational earthquake-induced building damage assessment using CNN-based direct remote sensing change detection on superpixel level

Yuanzhao Qing [a], Dongping Ming [a,b,*], Qi Wen [c], Qihao Weng [d], Lu Xu [a], Yangyang Chen [a], Yi Zhang [a], Beichen Zeng [a]

[a] School of Information Engineering, China University of Geosciences (Beijing), Beijing 100083, China
[b] Polytechnic Center for Natural Resources Big-data, Ministry of Natural Resources of China, Beijing 100036, China
[c] National Disaster Reduction Center, Ministry of Emergency Management, Beijing 100124, China
[d] Department of Land Surveying and Geo-Informatics, The Hong Kong Polytechnic University, Hong Kong, China

ARTICLE INFO

Keywords:
Building damage detection and assessment
Remote sensing
Convolutional neural network
Direct change detection
Earthquake damage index

ABSTRACT

Accurate and quick building damage assessment is an indispensable step after a destructive earthquake. Acquiring building damage information of the seismic area in a remotely sensed way enables a timely emergency response. Existing remote sensing building damage detection methods based on convolutional neural network (CNN) mainly need two-step processing or only use single post-event image, leading to low efficiency and inaccurate building boundary. Considering the practical needs of emergency rescue and post-disaster reconstruction, this study proposed a hierarchical building damage assessment workflow using CNN-based direct remote sensing change detection on superpixel level. First, vulnerable building areas close to the epicenter are extracted using extra feature enhancement bands (EFEBs) to narrow the extent of image processing. Then, fine scale building damage is detected in the extracted building areas based on a direct change detection method with pre-event superpixel constraint (PreSC) strategy to improve the precision and efficiency. Finally, a rapid remote sensing earthquake damage index (rRSEDI) is used to quantitatively assess the damage. Experimental results of the case study show that damaged buildings can be effectively and accurately localized and classified using the proposed workflow. Comparative experiments with single-temporal image and post-event segmentation further embody the superiority of the direct change detection. The damage assessment result matches the official report after Ludian earthquake, proving the reliability of the proposed workflow. For future natural hazard events, the workflow can contribute to formulating appropriate disaster management, prevention and mitigation policies.

1. Introduction

It is not possible for humans to accurately predict earthquakes, so proper and timely response and rescue are essential for mitigating the damages caused by such an inevitable and devastating calamity. For most of the earthquake casualties are associated with the severe damages to the buildings, rapid and efficient earthquake-induced building damage detection and assessment are crucial for rescue operations in a short period (Matin and Pradhan, 2021). Furthermore, the degree of damage to the buildings directly reflects the severity of the earthquake events, aiding the government in better decision-making and effective emergency response.

The conventional way to obtain information of building damage after earthquakes highly depends on ground investigation where both internal and external features of buildings are considered by experts. Although such detailed assessment is accurate, it is considered time-consuming, resource intensive and even dangerous (Gupta et al., 2019). Remote sensing images can make a very effective and rapid contribution towards inspecting the seismic area and exploiting the acquired information to organize emergency rescue due to their wide view (Weng, 2012; Vetrivel et al., 2018). Earthquake-induced damage mapping is one of the oldest applications of remote sensing, and it remains a topic of active research to date (Kerle, 2010). However, the current practice largely relies on emergency response crews and volunteers to annotate the damage manually, which is also known as visual interpretation. Despite of the high accuracy, visual interpretation costs more time and manpower. Therefore, there is a strong demand for building damage mapping to be an automatic task.

* Corresponding author at: School of Information Engineering, China University of Geosciences (Beijing), Beijing 100083, China.
E-mail address: mingdp@cugb.edu.cn (D. Ming).

https://doi.org/10.1016/j.jag.2022.102899
Received 3 April 2022; Received in revised form 26 June 2022; Accepted 27 June 2022
Available online 15 July 2022

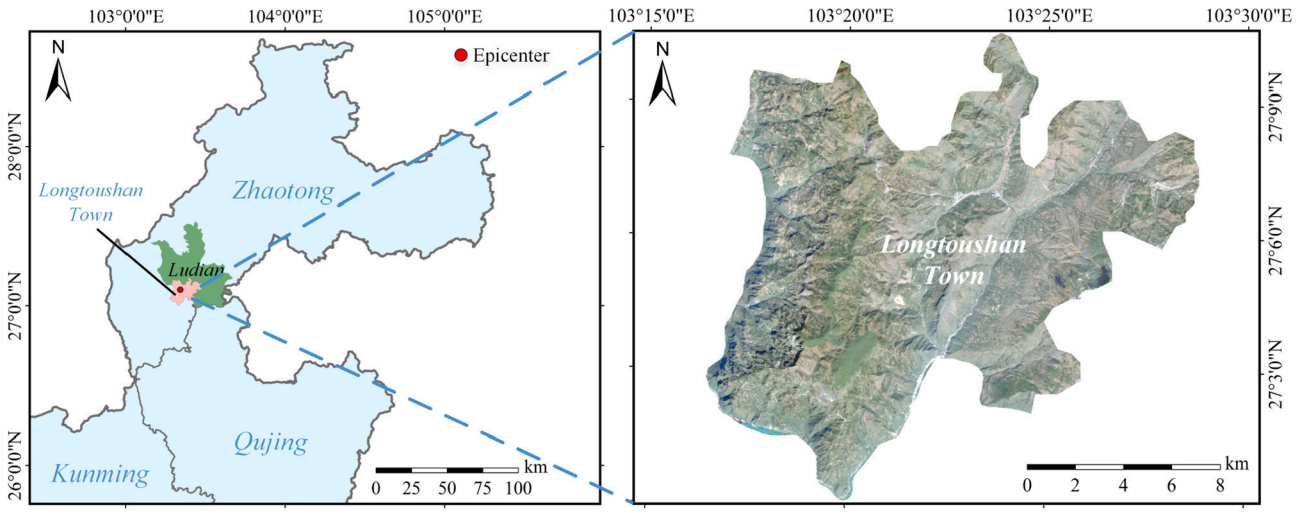

Fig. 1. Location and *Gaofen*-1 satellite image (2 m per-pixel) of the study area.

Table 1
Description of the data used in the study.

Type	Acquisition Time	Source	Spectral Bands	Spatial Resolution
Pre-earthquake	2013.09.29	GF-1	4-band multispectral	8 m
			1-band panchromatic	2 m
	2013	Google Earth	RGB	0.6 m
Post-earthquake	2014.08.07	UAV	RGB	0.2 m
Ancillary data	ASTER GDEM			30 m

Single-temporal methods that only use post-event images have been widely developed because of the easier acquisition and simple pre-processing of remote sensing data (Song et al., 2020). Although the assessing framework that only collecting and analyzing the images after earthquakes may be simple, the biggest problem of single-temporal methods is that they cannot locate the damaged buildings and detect the original boundary of them due to the lack of pre-event images and the scattered debris of collapsed buildings. Bitemporal assessment methods evaluate the damage by detecting meaningful changes using both pre- and post-earthquake images, which is also termed change detection (Plank, 2014). This kind of methods makes precise extraction of the boundary of damaged buildings available (Dong and Shan, 2013). Dubois and Lepage (2013) detected the building damage with high accuracy by comparing the texture and shape information of bitemporal QuickBird satellite images using object-based classification method after Haiti earthquake in 2010. To achieve an automatic learning of the

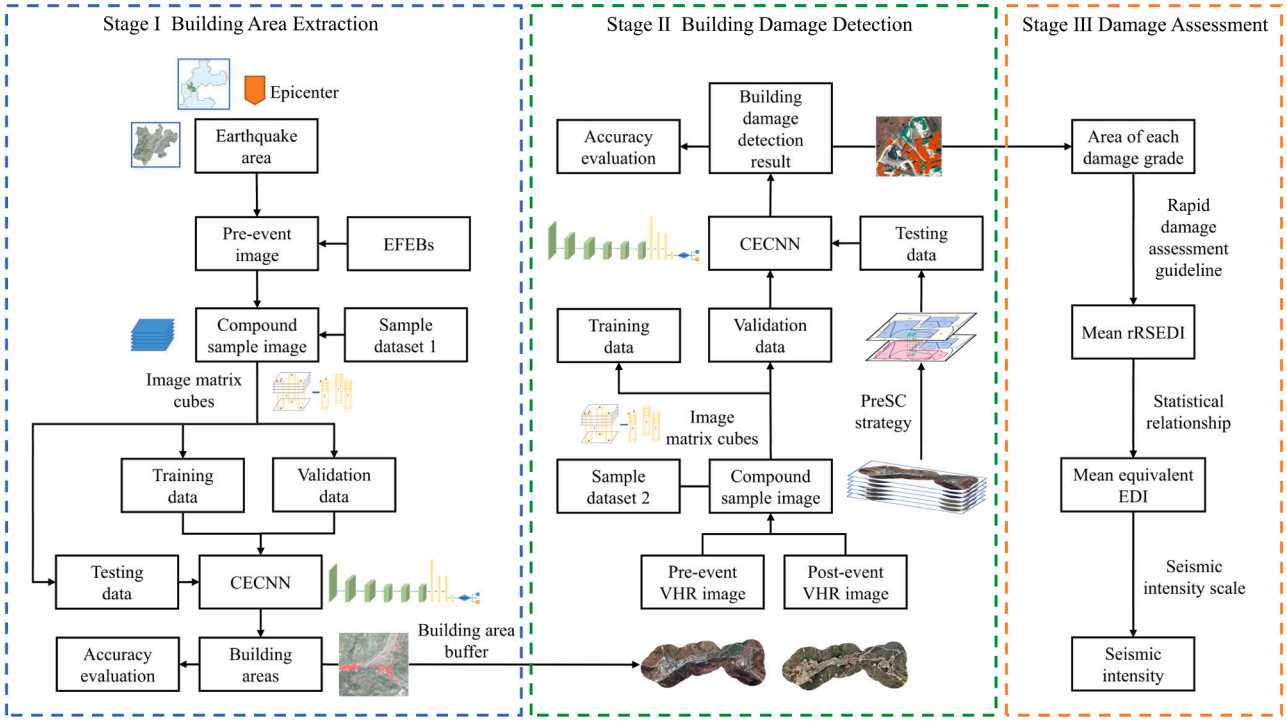

Fig. 2. Flowchart of the proposed workflow.

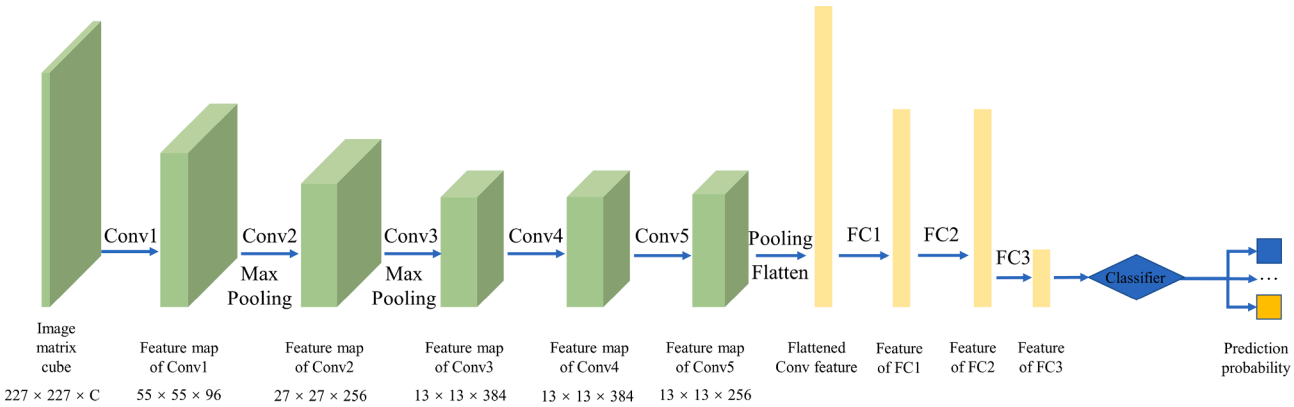

Fig. 3. The architecture of the introduced CECNN model. *C* represents the channel number.

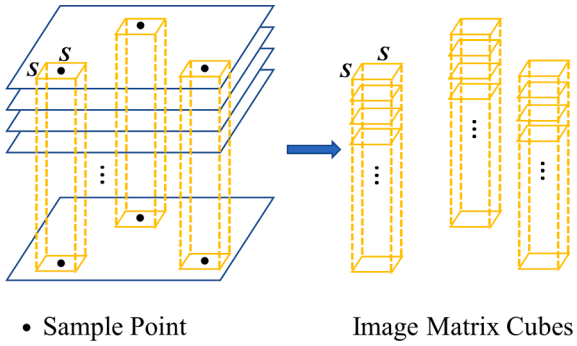

Fig. 4. Process of generating image matrix cubes.

required features from images, bitemporal machine learning (ML) models such as genetic algorithm (Mansouri and Hamednia, 2015) and artificial neural network (Syifa et al., 2019) were widely introduced to generate damage map. However, ML models generally ignore feature extraction and spatial pattern representation, resulting in limited complex feature expression abilities (Chen et al., 2021a).

In recent years, deep learning (DL) models, which learn high-level features from the raw data directly by extracting nonlinear relationships, is recognized as one of the most popular methods in extracting information from remote sensing images (Abdollahi et al., 2020; Dikshit et al., 2021). As the most state-of-the-art DL framework, convolutional neural networks (CNNs) have been widely used in geoscience domain (Lv et al., 2019; Chen et al., 2021b). CNN-based methods using pre- and post-earthquake images have been successfully and effectively applied in recent studies of building damage assessment. CNN-based building

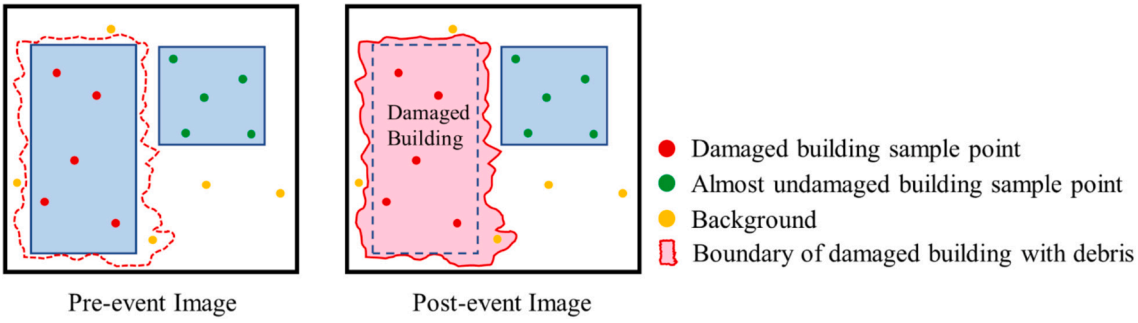

Fig. 5. Sample labelling based on change attributes for building damage detection.

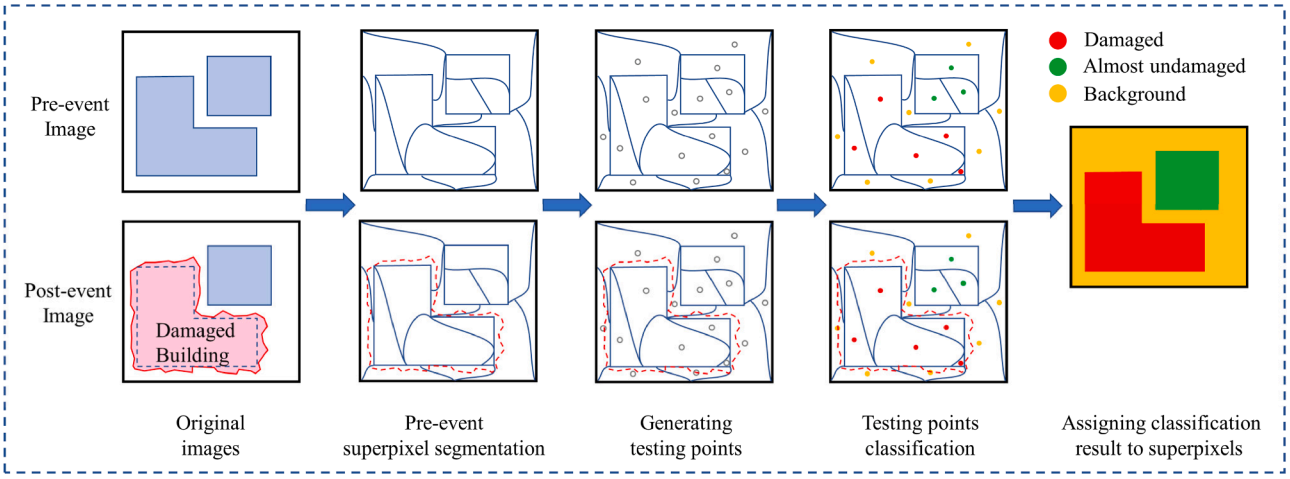

Fig. 6. Pre-event superpixel constraint (PreSC) straegy.

Table 2
Comparison of EMS98 and proposed classification scale of damage.

EMS98			Ours		
Grade Number	Grade Name	Description	Grade Number	Grade Name	Description
1	Negligible to slight damage	No structural damage, slight non-structural damage	1	Almost undamaged	No visible damage, the contour and texture of a certain building are almost the same as they were before the event.
2	Moderate damage	Slight structural damage, moderate non-structural damage	2	Damaged	Building with any types of damage that can be seen in vertical remote sensing images, including incompleteness of roof, collapse and totally destroyed.
3	Substantial to heavy damage	Moderate structural damage, heavy non-structural damage			
4	Very heavy damage	Heavy structural damage, very heavy non-structural damage			
5	Destruction	Very heavy structural damage			

damage detection mainly consists of building localization and damage grade classification. Conventional bitemporal CNN-based methods for building damage detection are mainly cascade network-based methods and Siamese network-based methods (Zheng et al., 2021). The cascade network-based approach is a two-step workflow using two different networks separately (Gupta et al., 2019). However, the building localization model and the damage classification model in the cascade network cannot share common knowledge with each other. To solve this problem, the Siamese network-based methods use the same network architecture to complete these two tasks by modeling them both as a pixel-level classification task using two fully convolutional networks (Shao et al., 2020; Valentijn et al., 2020). However, two different models need to be used in cascade network-based methods, while Siamese network-based methods also require a second training. They are both two-step methods, resulting in a waste of time and superposed errors. Therefore, it is of great importance to combine the two separate steps into a single workflow to fulfill the operational quick building damage assessment for emergency use.

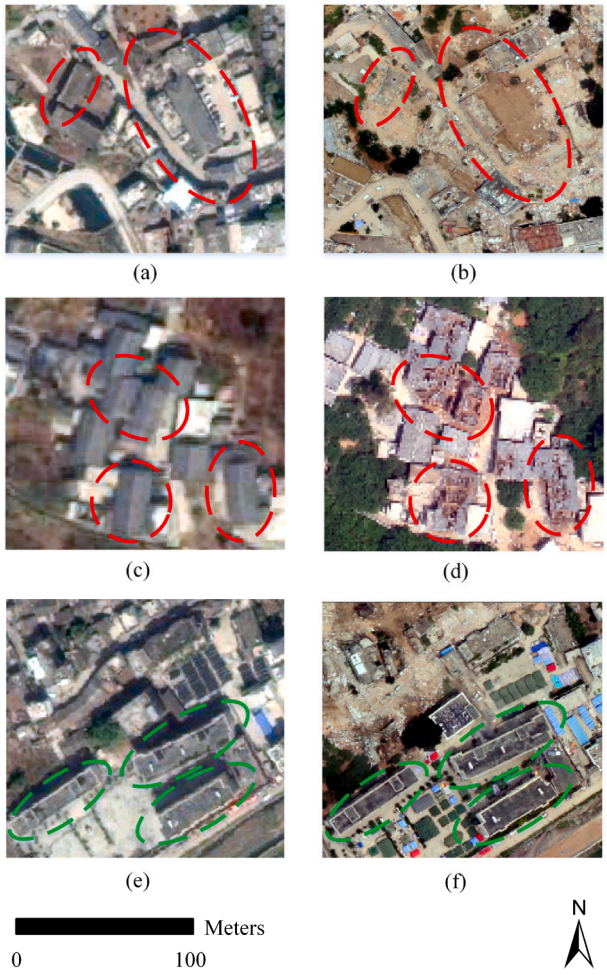

Fig. 7. The examples of *almost undamaged* buildings and *damaged* buildings in post-earthquake UAV image (0.6 m per-pixel). (a), (c) and (e) are pre-earthquake images; (b), (d) and (f) are post-earthquake images. Red circles in (a)-(d) are examples of *damaged* buildings; green circles in (e)-(f) are examples of *almost undamaged* buildings. (For interpretation of the references to colour in this figure legend, the reader is referred to the web version of this article.)

2. Case study and datasets

2.1. Study area

As shown in Fig. 1, this study highlights Longtoushan town, Ludian county, Yunnan, China. It was the most severely destroyed area after stricken by a M_S 6.5 earthquake that occurred at 16:30 GMT + 8 on August 3, 2014. The epicenter was located at approximately 27.10°N, 103.34°E, and the focal depth of this earthquake was 12 km (https://www.cea.gov.cn/cea/dzpd/dzzt/370016/index.html).

2.2. Datasets establishment

The description of the data used in the study is shown in Table 1. The

Table 3
The correspondence between EDI/rRSEDI and building damage grades.

Ground Investigation			Ours		
Grade	Grade Name	EDI	Grade	Grade Name	rRSEDI
1	No Damage	0.00	1	Almost Undamaged	0.01
2	Slight Damage	0.20	2	Damaged	0.75
3	Moderate Damage	0.40			
4	Heavy Damage	0.70			
5	Destruction	1.00			

Table 4
The simplified Chinese Seismic Intensity Scale (partial).

Seismic Intensity	Mean EDI
VI	0.00–0.11
VII	0.09–0.27
VIII	0.25–0.50
IX	0.48–0.69
X	0.67–0.91
XI	0.90–1.00
XII	1.00

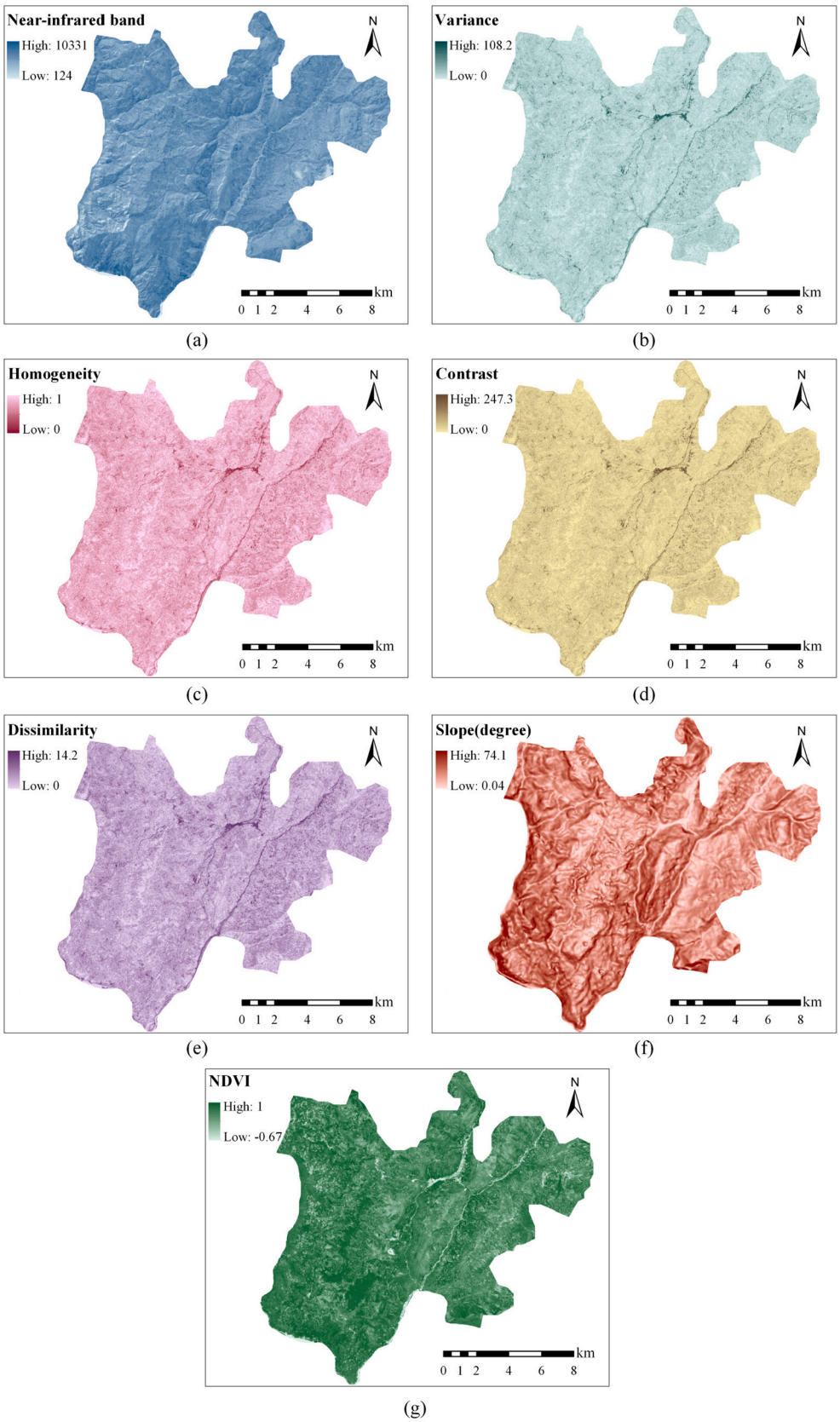

Fig. 8. EFEBs (2 m per-pixel) of the study area (Longtoushan Town) used in Stage *I*. (a) Near-infrared band. (b) Variance. (c) Homogeneity. (d) Contrast. (e) Dissimilarity. (f) Slope. (g) NDVI.

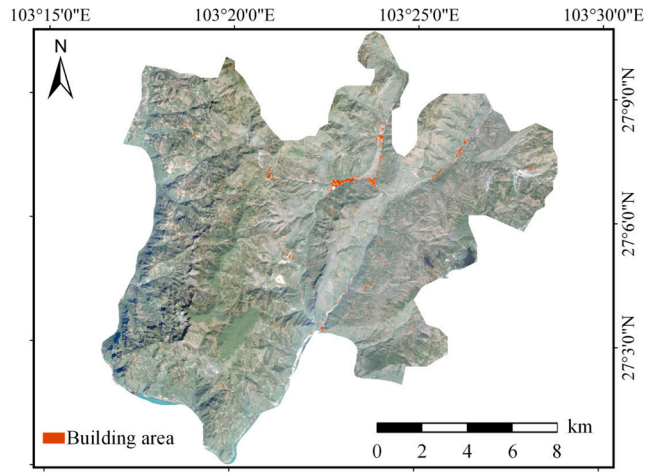

Fig. 9. The extracted building areas in pre-earthquake GF-1 image (2 m per-pixel) of Longtoushan Town.

Gaofen-1 (GF-1) image was provided by China Center for Resources Satellite Data and Application. The Advanced Spaceborne Thermal Emission and Reflection Radiometer Global Digital Elevation Model (ASTER GDEM) data was obtained from NASA Jet Propulsion Lab (JPL) and Japan's Ministry of Economy, Trade, and Industry (METI) (https://www.jspacesystems.or.jp/ersdac/GDEM/E/1.html).

In this study, two different datasets were established. Sample *Dataset* 1 is used for building area extraction and sample *Dataset* 2 is for fine scale building damage detection using bitemporal images. The samples used for CNN model were represented by point vector instead of polygon, making the labeling process timely.

3. Methodology

3.1. Stratified workflow

Considering the requirements of practical applications of emergency response, building damage is detected hierarchically by a top-down process. The methodology flowchart of the proposed operational workflow is shown in Fig. 2. The workflow consists of three stages.

(1) Stage *I*: Building Area Extraction.

The aim of Stage *I* is to extract building areas which are most likely to be affected by an earthquake in a coarse scale. After extracting building areas in a meizoseismal region, decision-makers and rescue teams in site can easily resize the post-event image or send UAVs to these areas and collect VHR images to narrow the processing scope and find whether there are damaged buildings. By doing so, the efficiency of the whole workflow is improved.

(2) Stage *II*: Building Damage Detection.

Fine scale building damage detection is conducted based on the building areas extracted in Stage *I* using a direct change detection.

(3) Stage *III*: Damage Assessment

The reginal seismic intensity is calculated based on the roof surface area of buildings in different damage grades determined in Stage *II* and the proposed rapid damage assessment guideline. According to the relationship between earthquake damage index and seismic intensity, the damage of a certain area can be assessed.

3.2. Multi-band image analysis

When using remote sensing data for geoscience research, we often expect to mine as much thematic information as possible from images, and the rich band information in remote sensing image is the premise and guarantee to achieve this goal. In addition to the rich multispectral bands of the image, multi-temporal images, texture feature layers and band calculation results such as vegetation index can also be superimposed into the CNN model as new channels. Those bands are defined as extra feature enhancement bands (EFEBs) in this study.

To fulfill the technical need of multi-band analysis, the conventional CNN model needs to be modified. In this study, the pretrained channel-expanded CNN (CECNN), whose basis is AlexNet (Krizhevsky et al., 2012), modified by Chen et al. (2021a, 2021b) was introduced as the basis of CECNN model for multi-band sample image analysis (shown in Fig. 3).

In addition, training samples need to be input into CNN in the form of images. Image matrix cubes were used for training and testing of CECNN model (Chen et al., 2021a, 2021b). The process of generating image matrix cubes is given in Fig. 4. The multi-band compound sample image was clipped into $S \times S \times B$ image matrix cubes by sample points. S stands for the resize parameter of CNN dataset and B is the band number of image. Each clipped image matrix shares the same geometric center with a corresponding sample point.

3.3. Direct change detection

Building damage detection can be regarded as "one-to-n" semantic change detection, that is, the intact buildings before the earthquake become the buildings with different types of damage after the earthquake. In Stage *II*, building damage detection was implemented as a CECNN-based single-step direct change detection on superpixel level by using the following strategies.

3.3.1. Sample labelling based on change attributes

The sample points are generated based on landcover or object types from both anterior and posterior images separately in conventional change detection, leading to a lack of change information. In Stage *II*. We innovatively added the change information into samples to fulfill a direct single-step damage detection. As illustrated in Fig. 5, sample points were selected based on the changes of buildings which represent different damage grades after earthquakes. In this study, the changes of each building area were divided into 3 categories: from intact buildings to damaged buildings, intact buildings before the earthquake are still basically in a good situation after the earthquake, and other changes involve background features. The above 3 types of changes correspond to *almost undamaged building*, *damaged building* and *background* classes defined in Stage *II*.

3.3.2. Pre-event superpixel constraint strategy

In order to get accurate building boundaries of the original buildings for clear illustration and to improve the efficiency, pre-event superpixel constraint (PreSC) strategy was proposed for direct building damage detection. PreSC is an object-based image analysis (OBIA) strategy for delineating boundaries of buildings and recognize the damage grade of each building instance simultaneously.

As shown in Fig. 6, superpixel segmentation is conducted only on pre-earthquake image for OBIA, so that the original boundaries of buildings before the earthquake can be preserved to constrain the damage detection process. All the superpixels formed a polygon shapefile and every band of the compound sample image is analyzed by CECNN under the constraint of same superpixels. Next, a testing sample point is generated at the geometric center of each superpixel, and a corresponding image matrix cube is also generated for classification. Because of the high homogeneity of the superpixel object, the classification result of the central point can represent the category of the

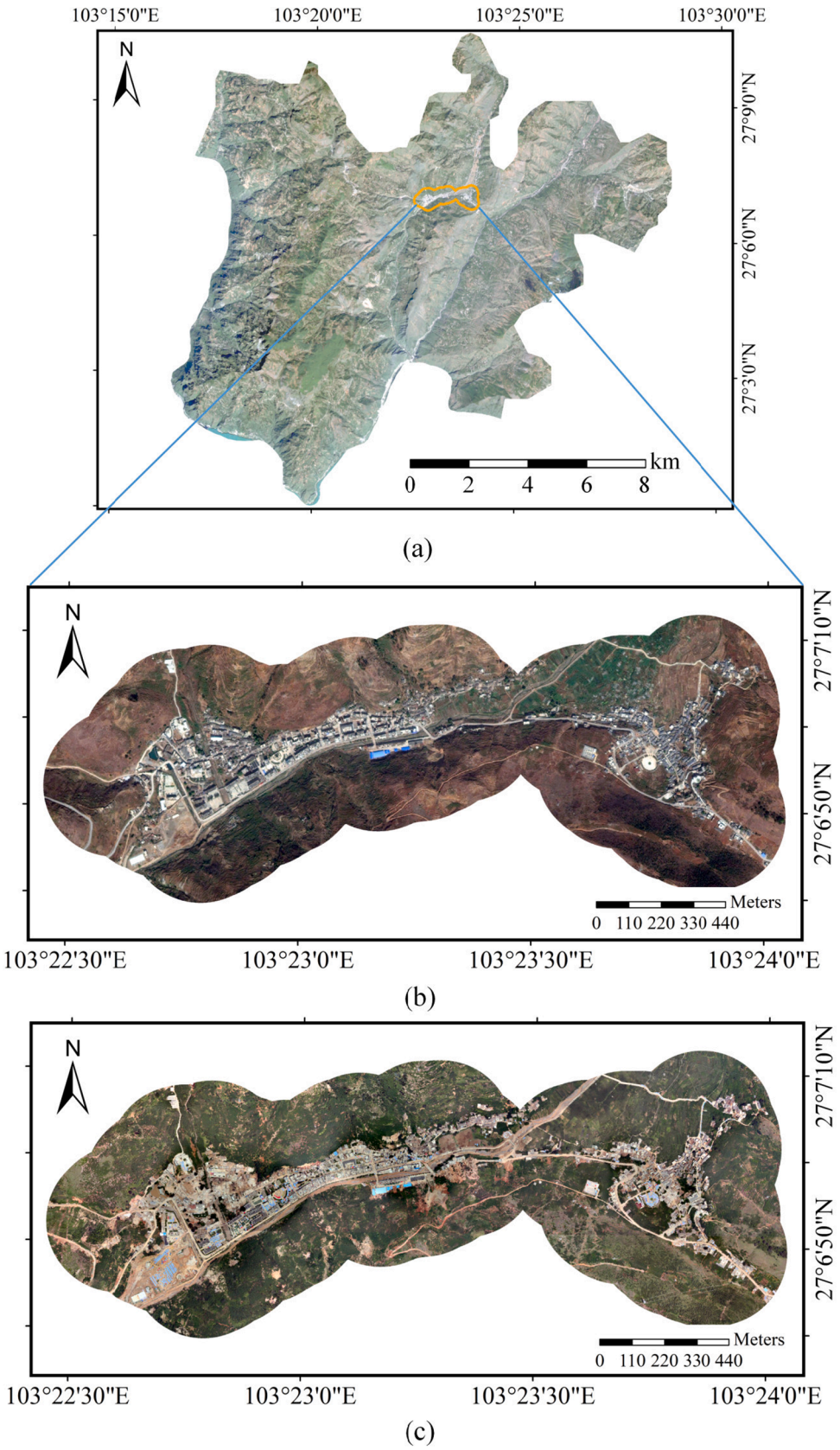

Fig. 10. Image preprocessing for building damage detection. (a) Buffer of the downtown area of Longtoushan Town. (b) Clipped pre-earthquake Google Earth image. (c) Clipped post-earthquake UAV image.

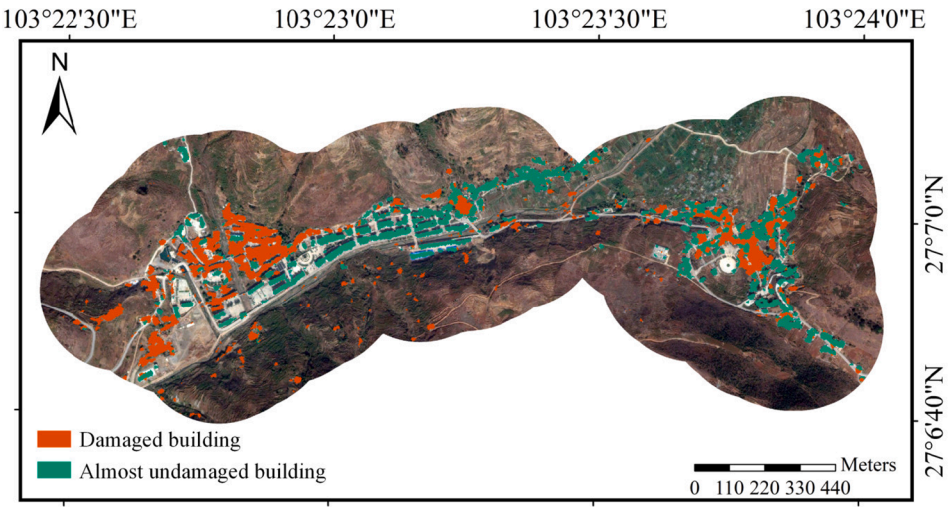

Fig. 11. Building damage detection result of the downtown area of Longtoushan Town (shown in pre-earthquake Google Earth image).

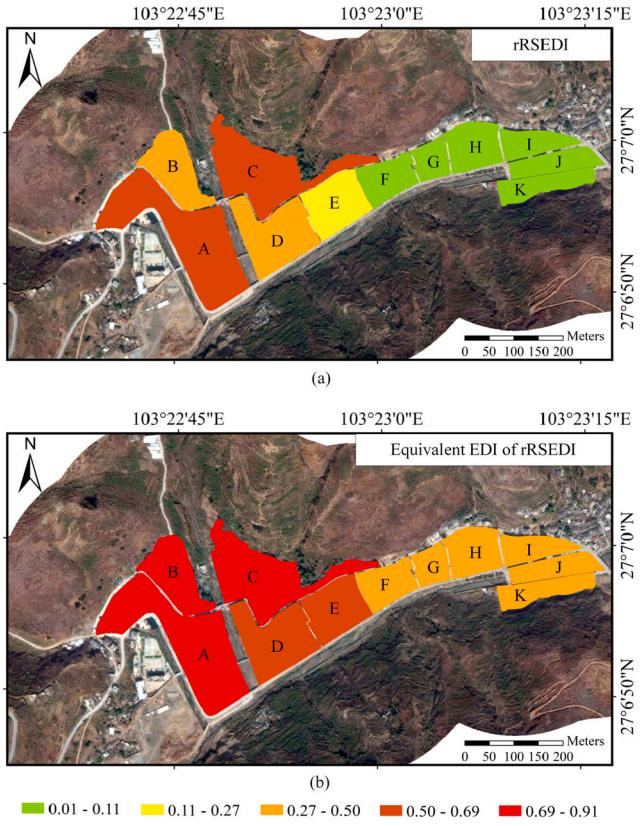

Fig. 12. Damage assessment result of blocks in downtown area. (a) rRSEDI. (b) Equivalent EDI of rRSEDI.

superpixel object. Finally, the building damage detection results after the earthquake can be obtained.

3.4. Rapid damage assessment guideline

3.4.1. Building damage grade classification

There are several damage level classification guidelines proposed for building damage assessment (Cotrufo et al., 2018; Monfort et al., 2019). For remote sensing assessment, some detailed damages on the wall and pancake damage (i.e., seen intact in vertical image) can hardly be detected under most of the existing damage grade classification guidelines using remote sensing images. As shown in Table 2, compared with The European Macroseismic Scale (EMS98) (Grünthal, 1998), we only separated the buildings into two grades to satisfy the demand of urgent remote sensing assessment after an earthquake. Fig. 7 illustrates the examples of buildings categorized into *almost undamaged* grade and *damaged* grade in this study.

3.4.2. Rapid remote sensing earthquake damage index

Seismic intensity measures the impact and ground vibration caused by earthquakes. The correspondence between the earthquake damage index (EDI) and building damage grades and the correspondence between reginal mean EDI and seismic intensity defined by The Chinese Seismic Intensity Scale are shown in Table 3 and Table 4, respectively. Therefore, the comprehensive evaluation of seismic intensity can be carried out by calculating the mean EDI.

The EDI of buildings can also be determined by remote sensing (Wang et al., 2015). In this study, the rapid remote sensing EDI (rRSEDI) was proposed and used for buildings (see Table 3). There might be invisible damage among the *almost undamaged* buildings and all kinds of visible *damaged* buildings, including slight, moderate, heavy damage, etc., are hard to be classified using remote sensing images. For this reason, the detailed damage grades were regarded as one category, the rRSEDI of *almost undamaged* building and *damaged* building were set to 0.01 and 0.75 respectively.

However, because of the limitation of remote sensing earthquake damage detection, RSEDI differs from EDI based on ground investiga-

Table 5
Damage assessment result of blocks in downtown area.

Block	A	B	C	D	E	F	G	H	I	J	K	Average
D_A^{RS}	0.58	0.46	0.69	0.42	0.20	0.03	0.07	0.04	0.01	0.04	0.09	0.24
D_A^{G}	0.80	0.72	0.87	0.69	0.51	0.34	0.38	0.35	0.32	0.40	0.35	0.52
Seismic Intensity	*X*	*X*	*X*	*X*	*IX*	*VIII*	*VIII*	*VIII*	*VIII*	*VIII*	*VIII*	*IX*

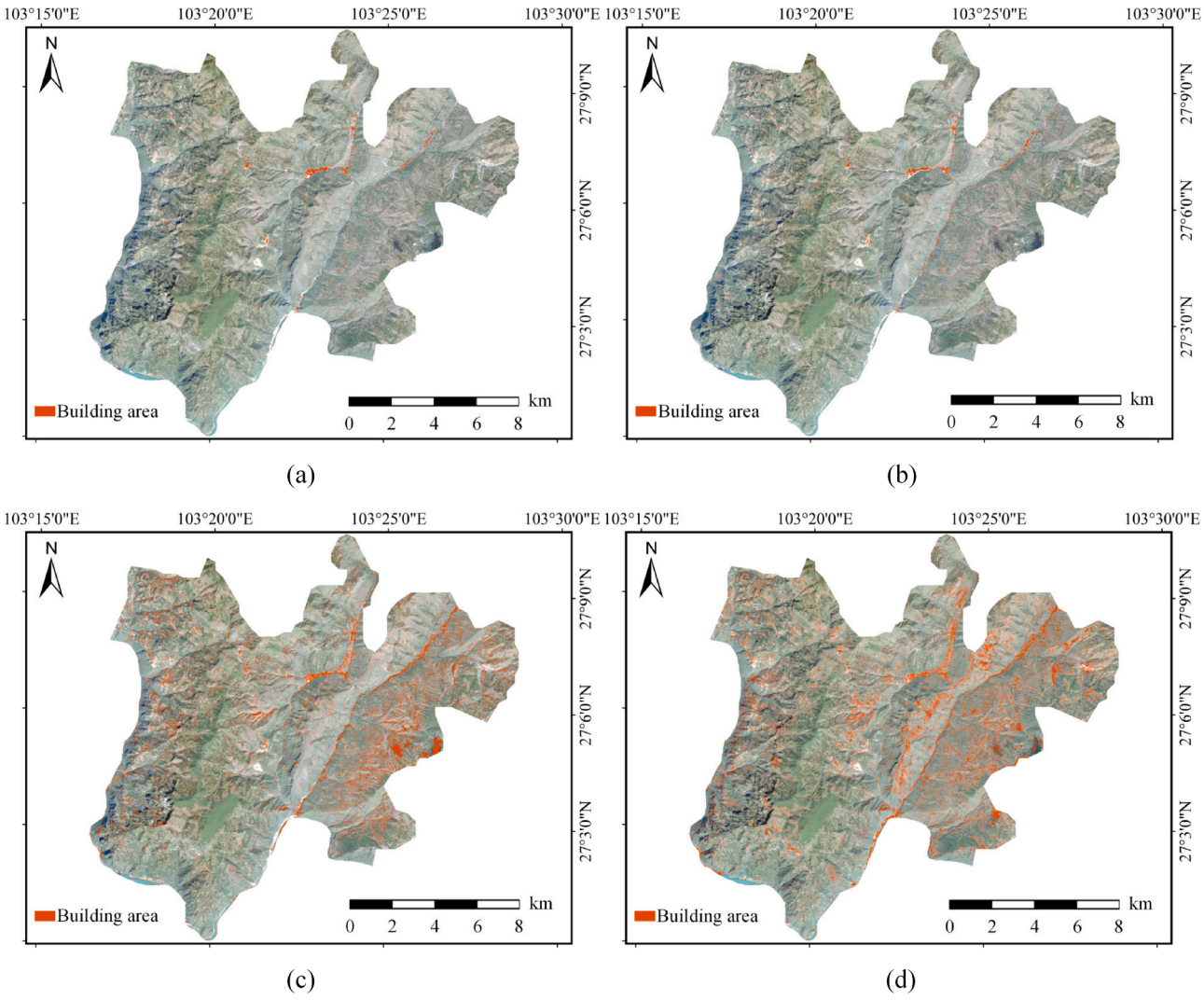

Fig. 13. Building area extraction results in GF-1 image using different methods. (a) CECNN-EFEB (Ours). (b) CECNN. (c) SVM-EFEB. (d) SVM.

tion. Dou et al. (2012) discovered a quantitative relationship between mean RSEDI and mean EDI determined by ground investigation through sampling survey and statistical analysis, so that the RSEDI in other non-surveyed sites in the earthquake disaster area can be transformed into an equivalent EDI. The effectiveness of this relationship was verified by them after the 2008 Wenchuan earthquake and the 2010 Yushu earthquake occurred in China. The polynomial fitting relation is

$$D_A^G = -0.405(D_A^{RS})^2 + 1.092D_A^{RS} + 0.306 \quad (1)$$

where D_A^G represents the equivalent EDI of rRSEDI, while D_A^{RS} denotes the RSEDI. In the proposed workflow, the mean rRSEDI is used to calculate the equivalent EDI based on above relationship. For an investigation area, a mean rRSEDI based on the area of the roof surface of buildings is defined as

$$D_A^{RS} = \frac{\sum_{j=1}^{2} d_j A_j}{\sum_{j=1}^{2} A_j} \quad (2)$$

where D_A^{RS} represents the proposed mean rRSEDI. d_j stands for the rRSEDI of buildings at damage grade j (j = 1,2). A_j represents the area of the roof surface of buildings at damage grade j (j = 1,2). In this way, the seismic intensity can be evaluated by remote sensing based on the transformed mean rRSEDI and its corresponding relationship with seismic intensity.

3.5. Accuracy evaluation

Building area extraction and building damage detection results were evaluated with respect to the labeled ground truth by calculating overall accuracy (OA), Kappa coefficient (Kappa), intersection over union (IoU), Precision, Recall, and F1-Score. The calculation formulae are as follows:

$$OA = \frac{N_T}{N} \quad (3)$$

$$Kappa = \frac{N\sum_{i=1}^{r} x_{ii} - \sum_{i=1}^{r}(x_{i+}x_{+i})}{N^2 - \sum_{i=1}^{r}(x_{i+}x_{+i})} \quad (4)$$

$$Precision = \frac{TP_{area}}{TP_{area} + FP_{area}} \quad (5)$$

$$Recall = \frac{TP_{area}}{TP_{area} + FN_{area}} \quad (6)$$

$$F1 - Score = 2 \times \frac{Precision \times \text{Recall}}{Precision + \text{Recall}} \quad (7)$$

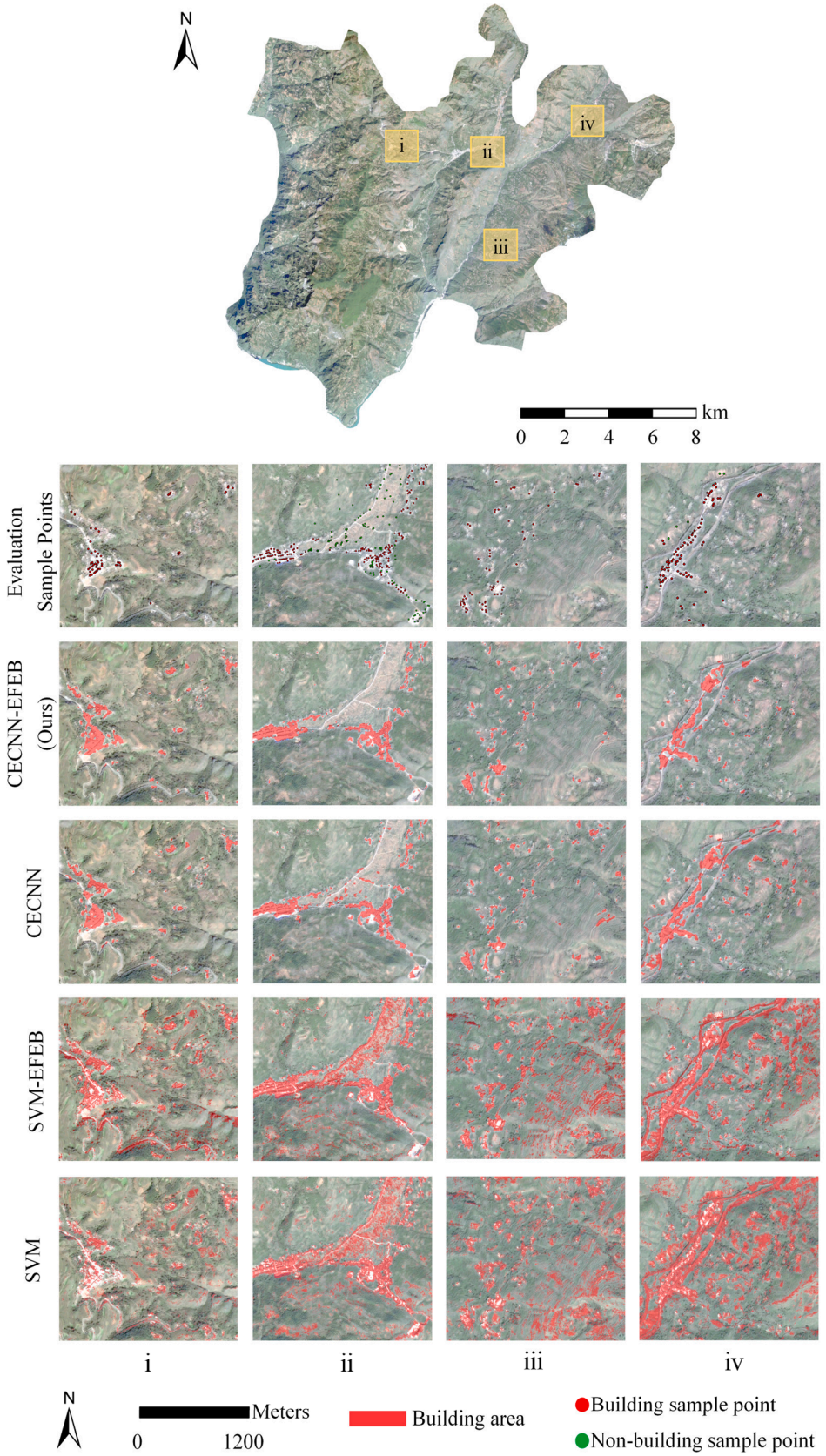

Fig. 14. Zoomed views of building area extraction results in GF-1 image using different methods.

Table 6
Evaluation result of building area extraction based on confusion matrix.

		Prediction result				OA(%)	Kappa
			Building	Non-building	Sum		
CECNN-EFEB (Ours)	Ground truth	Building	822	178	1000	**89.2**	**0.784**
		Non-building	38	962	1000		
		Sum	860	1140	2000		
CECNN		Building	830	170	1000	87.7	0.755
		Non-building	75	925	1000		
		Sum	905	1095	2000		
SVM-EFEB		Building	825	175	1000	78.9	0.579
		Non-building	246	754	1000		
		Sum	1071	929	2000		
SVM		Building	611	389	1000	63.1	0.261
		Non-building	350	650	1000		
		Sum	961	1039	2000		

$$IoU = \frac{A_p \bigcap A_r}{A_p \bigcup A_r} \tag{8}$$

where N_T and N denotes the number of correctly classified sample points and total number of sample points, respectively. r represents the class number. x_{ii} is the sample number of row i and column i in the confusion matrix. x_{i+} and x_{+i} represent the total sample number of row i and column i in the confusion matrix, respectively. TP_{area} and TN_{area} denote the roof surface area of correctly predicted and incorrectly predicted buildings in a certain damage grade, respectively. FP_{area} and FN_{area} are the mispredicted correct and incorrect roof surface area of buildings in a certain damage grade. A_p and A_r represent the predicted area and true area of the roof surface of buildings respectively in each damage grade.

4. Experiments and results

Experiments were carried out on Windows 10 with 3.6 GHz Core i7-7700 and NVIDIA GeForce GTX 1080. TensorFlow-GPU 1.3.0 was selected as DL platform. The results are shown in this section.

4.1. Building area extraction with EFEBs

The epicenter was located in Longtoushan Town, Ludian county, so the region of Longtoushan was selected as a high-risk area. In this region, original building areas were extracted firstly in a coarse scale using 7 EFEBs based on pre-event image. One near-infrared band, four grey-level co-occurrence matrix (GLCM) (Haralick et al., 1973) textural features bands (i.e., variance, homogeneity, contrast and dissimilarity), one slope band calculated by using the ASTER GDEM data and one normalized difference vegetation index (NDVI) band were selected as EFEBs, forming a 10-band compound image along with three RGB bands. The EFEBs used for Stage *I* are shown in Fig. 8.

Based on GF-1 image, 2000 building sample points and 2000 non-building sample points were selected from Wenping town just next to Longtoushan through visual interpretation to ensure the independency, forming *Dataset* 1. When generating image matrix cubes, the resize parameter S was set to 71 based on trial-and-error to create $71 \times 71 \times 10$ image matrix cubes. 80% of these cubes were used for model training while the rest 20% of them composed validation set. In stage *I*, prediction process of optimized CECNN was executed based on pixels. Specially, NDVI was used to improve computational efficiency by removing high vegetation coverage areas. The extracted building areas are shown in Fig. 9.

4.2. Building damage detection

In this study, the downtown area of Longtoushan town was extracted and selected as an example region to test the performance of the proposed direct change detection for building damage.

First, 250-meter buffer was created for each extracted building area. Two buffers covering downtown area were selected and dissolved, forming a single downtown buffer. As shown in Fig. 10, the UAV image collected 4 days after the Ludian earthquake and the Google Earth image collected before the event were resampling to 0.6 m per-pixel and were clipped by the downtown buffer as compound sample image. Then, the clipped pre-event image was segmented using Superpixels Extracted via Energy-driven Sampling (SEEDS) (Van den Bergh et al., 2015) with a scale parameter selected based on trial-and-error to guarantee high homogeneity for a single type of change in each superpixel object. 1300 sample points were selected for each class in *Dataset* 2 based on the VHR image pair mentioned above, which were strictly cross-checked by several interpreters.

The resize parameter S was also set to 71 to create $71 \times 71 \times 6$ image matrix cubes. The proportions of image cubes used for CECNN model training and validation were the same as Stage *I* in Section 4.1. Shown in Fig. 11, with the help of the proposed direct change detection, the damages of buildings were detected. Specially, only two classes of building grades were showed in damage maps except *background* to emphasize the information of interest.

4.3. Damage assessment

In this study, the rRSEDI D_A^{RS} was calculated based on the damage grade classification result by Formula 2, and was transformed into the equivalent EDI D_A^G through Formula 1. As shown in Table 4, the D_A^{RS} of the entire downtown area is 0.36, the equivalent EDI D_A^G is 0.65. According to The Chinese Seismic Intensity Scale, the seismic intensity of downtown area in Longtoushan town is IX after the Ludian earthquake. To better understand the damage, the downtown area was divided into 11 blocks based on main roads. As can be seen in Fig. 12 and Table 5, Block A, B, C and D were seriously damaged with an intensity of *X*. All of these blocks share an average seismic intensity of IX.

5. Discussion

5.1. Effectiveness of EFEBs

In order to evaluate the effectiveness of EFEBs based on CECNN, The SVM machine learning model was selected to make a comparison. 2000 evaluation points were selected and labelled for accuracy evaluation. As can be seen in Figs. 13-14 and Table 6, the CECNN model with EFEB achieved an OA of 89.2% and a Kappa of 0.784, which is 1.5% and 0.029 higher than the one which only used RGB bands. The proposed method achieved significantly higher accuracy. When innovatively using EFEBs,

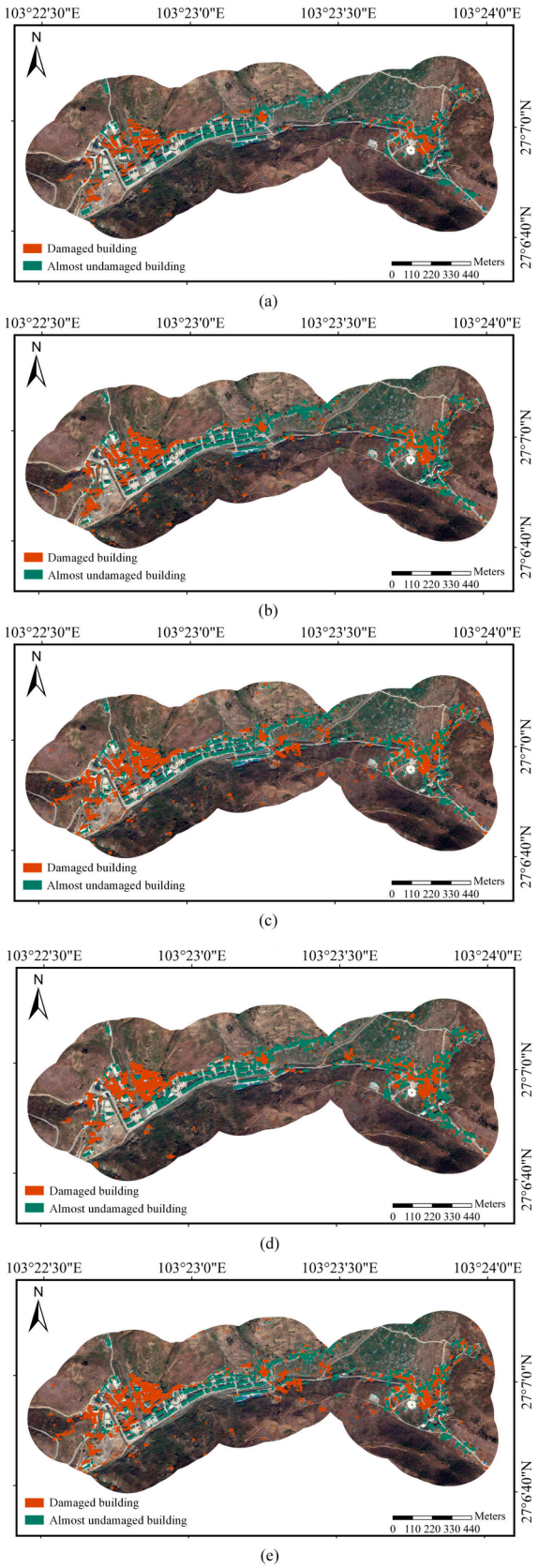

Fig. 15. Results of building damage detection and damage grade classification using different method combinations (shown in pre-earthquake Google Earth image). (a) Ground truth. (b) Direct change detection + PreSC (Ours). (c) Direct change detection. (d) AlexNet + PreSC. (e) AlexNet.

the textural and topographical features have been greatly enhanced. Four GLCM textural features provide richer textural features. The slope layer can significantly differentiate the flat building areas from areas with large slope such as bare land on the mountain or landslide area. NDVI helps remove areas of low vegetation cover areas. Therefore, there are much less misclassified pixels in the classification result of the proposed method comparing with the method which conventionally uses RGB bands, proving the effectiveness of EFEBs.

Therefore, more EFEBs can provide important additional information to help CECNN with multi-band image analysis for higher efficiency and accuracy.

5.2. *Effectiveness of the direct damage detection*

The performance evaluation of the proposed direct bitemporal damage detection was conducted by comparing whether to use the direct change detection method and whether to use PreSC strategy based on the ground truth of building damage precisely labelled manually on the pre-event image. Figs. 15-16 show the building damage detection results of each method combination. The roof surface area of buildings before the earthquake can be well preserved and the damage area can be effectively located and classified into different damage grades. It can be summarized from the figures and Table 7 that the direct change detection with PreSC strategy outperforms other method combinations for the highest consistency of building boundary and highest damage grade classification accuracy. The proposed method achieved an IoU of 0.522 and a comprehensive F1-Score of 0.686, which is 0.101 and 0.096 higher than the method only used AlexNet to process 3-band post-earthquake image without PreSC strategy.

The application of CECNN-based direct bitemporal damage detection improves the detection accuracy and efficiency for emergency after earthquake by integrating building localization and damage classification into a unified stage. The sample labelling based on change attributes simplifies the complex change detection into a single-step multi-classification task in terms of the damage grade, while the proposed PreSC strategy ensures the feasibility of damage grade detection.

Although the visualized performance of the proposed method in building damage detection is quite acceptable, it seems that the IoU and F1-Score are not very satisfactory. Due to the limited spatial resolution and different source of remote sensing images used in this study, most of the buildings in Longtoushan town, especially the bungalows, cannot be segmented into separate ones, leading to a decreased accuracy of building boundary.

The accuracy evaluation result can be greatly affected by the choice of evaluation method. To verify the effectiveness of the proposed method in building damage detection, an additional evaluation based on stratified sampling was conducted. 1000 evaluation points were generated randomly for each class. The result is illustrated in Fig. 17 and Table 8. Our proposed method achieved an OA of 88.5% and a Kappa of 0.828, which is 6.4% and 0.096 higher than method only use post-earthquake image without pre-event PreSC strategy. The accuracy is quite acceptable, proving the effectiveness of the direct change detection.

5.3. *Reliability of the damage assessment result*

With the help of the proposed rapid damage assessment guideline, the overall seismic intensity of the downtown area of Longtoushan town can be determined as IX. The result matches the assessment result conducted by China Earthquake Administration in August 7, 2014 (https://www.gov.cn/xinwen/2014–08/07/content_2731360.htm), which proves the reliability of the proposed rRSEDI, the damage scale and the whole rapid building damage assessment workflow.

Although the detailed damage grades based on ground investigation were ignored, the remote sensing assessment result is enough for decision-maker and rescue team to understand where the damaged

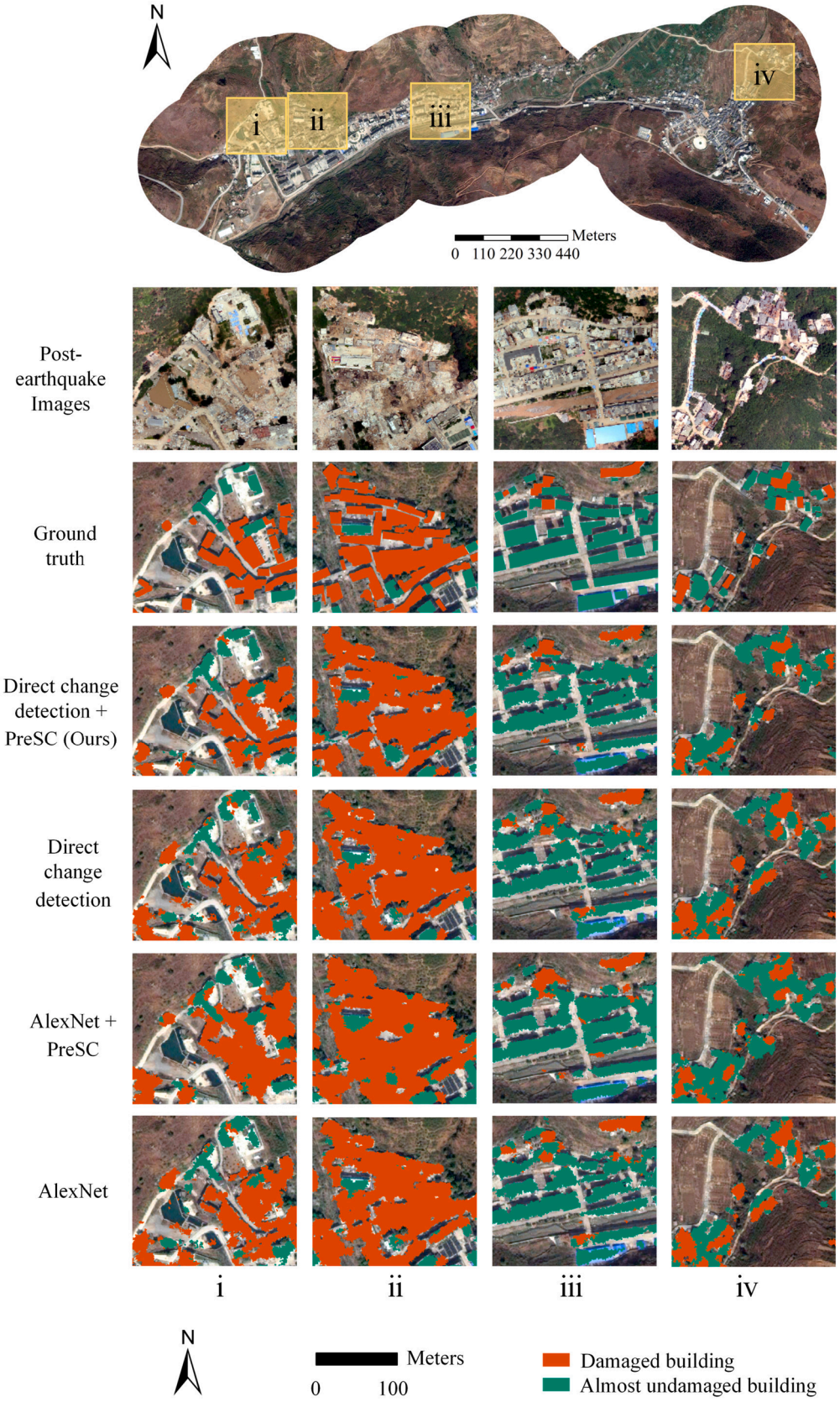

Fig. 16. Zoomed results of building damage detection using different method combinations (shown in pre-earthquake Google Earth image).

Table 7
Evaluation result of different damage detection method combinations.

Method combination	IoU	Recall	Precision	F1-Score
Direct change detection + PreSC (Ours)	**0.522**	**0.840**	**0.582**	**0.686**
Direct change detection	0.459	**0.840**	0.503	0.629
AlexNet + PreSC	0.422	0.777	0.489	0.591
AlexNet	0.421	0.774	0.489	0.590

buildings located and what the seismic intensity of a certain area is. Then, the emergency management department can formulate pertinent disaster relief plans for each region with different seismic intensity and organize efficient post-disaster reconstruction.

5.4. Timeliness estimation

To illustrate the efficiency of our workflow, the timeliness analysis was conducted based on multiple experiments. As shown in Fig. 18, under the premise that bitemporal images have been obtained, Stage *I* needs about 1 h (including data preprocessing), Stage II costs about 30 min, while Stage III needs approximately 5 min. It only takes about 1.5 h to get damage detection and final assessment result.

Table 8
Evaluation result of different damage detection method combinations based on stratified sampling.

Method	OA (%)	Kappa
Direct change detection + PreSC (Ours)	**88.5**	**0.828**
Direct change detection	86.4	0.797
AlexNet + PreSC	82.1	0.732
AlexNet	82.1	0.732

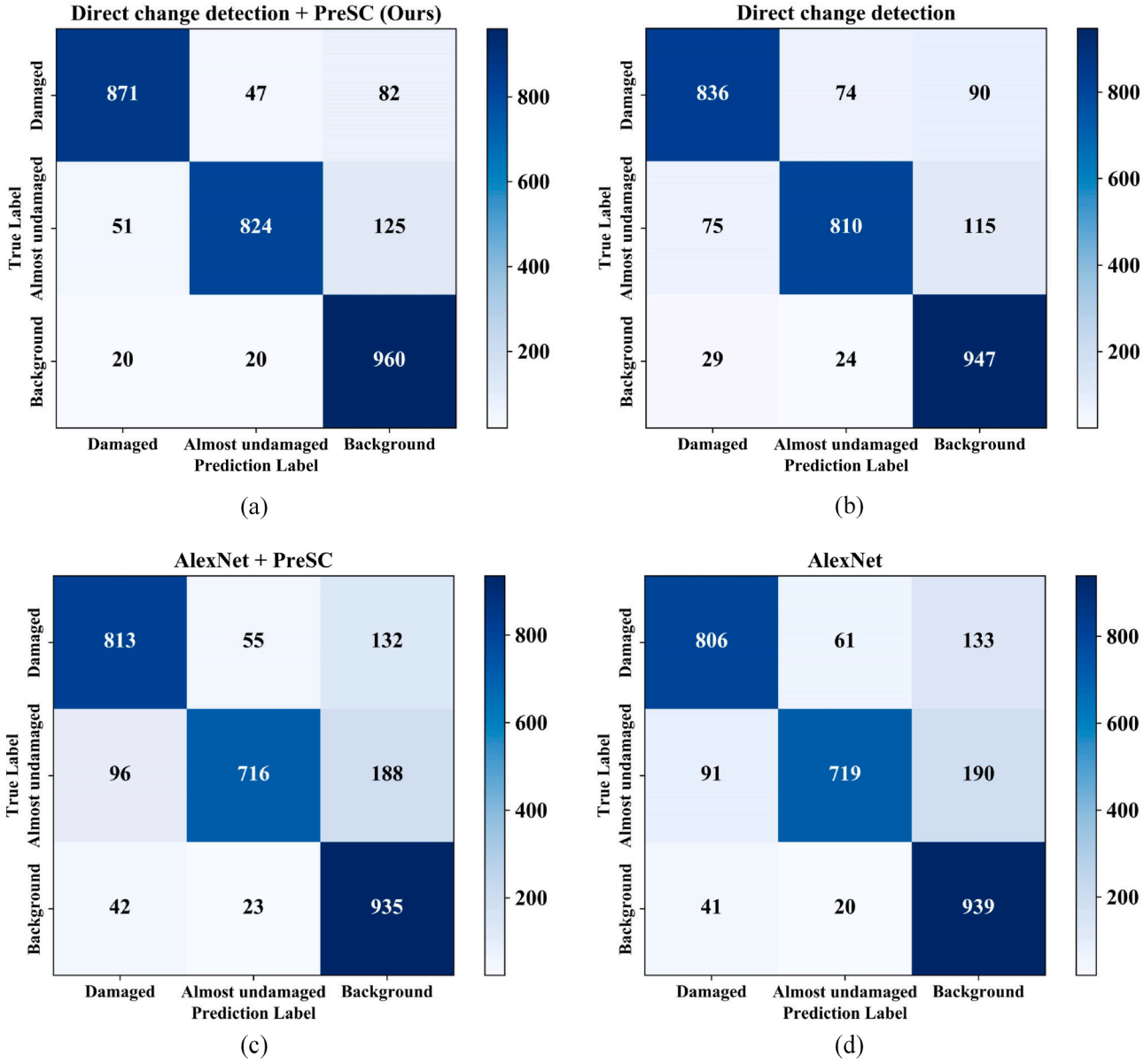

Fig. 17. Confusion matrixes of different damage detection method combinations. (a) Direct change detection + PreSC (Ours). (b) Direct change detection. (c) AlexNet + PreSC. (d) AlexNet.

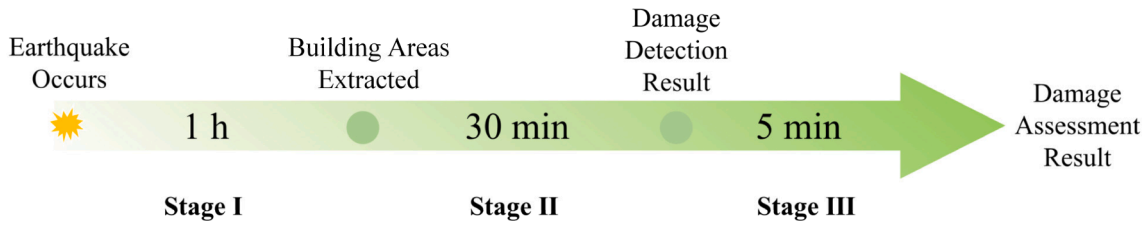

Fig. 18. Timeline of the proposed workflow.

However, the processing time is only estimated under certain conditions, and factors such as different seismic areas and different experimental equipment may affect the efficiency of evaluation.

6. Conclusions

In this study, an operational earthquake-induced building damage assessment using CNN-based direct remote sensing change detection on superpixel level was proposed. Based on experimental results and analysis, the conclusions can be drawn as follows.

(1) The EFEBs and CECNN ensure the multi-band image analysis for significantly improving the accuracy of building area extraction and accelerating the process of the damage assessment workflow.
(2) The proposed direct change detection innovatively integrates building localization and damage classification into a unified process, which improves the efficiency and accuracy of building damage detection.
(3) The rapid damage assessment guideline used in this study, including simplified damage scale and the rRSEDI, avoids inaccurate subdivision of earthquake damage grades and improves the efficiency and reliability of remotely sensed post-earthquake emergency assessment.

In conclusion, the newly proposed operational earthquake-induced building damage assessment framework with a direct change detection is a promising workflow to assess building damage with high timeliness and precision. Achievements of this study can not only help government develop a disaster response strategy, but also aids decision-makers in better designing buildings and infrastructure which can withstand destruction in future seismic events. In addition, as core method of the workflow, direct change detection can also be introduced to other domains of geoscience application such as semantic change detection for natural resources monitoring.

Nevertheless, the large disaster remote sensing datasets need to be established to improve the transferable of the CNN model. The statistical relationship between RSEDI and the EDI determined by ground investigation used in this study has certain particularity. So, more ground investigation data of earthquake disaster should be taken into consideration to form a more reliable regression relation between rRSEDI and EDI in further study. Besides, in our damage assessment guideline, moderate damage grades are ignored for emergency use purpose because of the limited resolution and vertical viewing angle of remote sensing, which is a key problem for further study. There is an urgent need for designing an internationally accepted damage assessment guideline to be followed in creating a comprehensive building damage database.

CRediT authorship contribution statement

Yuanzhao Qing: Conceptualization, Methodology, Writing – original draft. **Dongping Ming:** Project administration, Supervision, Writing – review & editing. **Qi Wen:** Investigation. **Qihao Weng:** Supervision. **Lu Xu:** Supervision, Writing – review & editing. **Yangyang Chen:** Software, Resources. **Yi Zhang:** Formal analysis, Investigation. **Beichen Zeng:** Data curation, Visualization, Validation.

Declaration of Competing Interest

The authors declare that they have no known competing financial interests or personal relationships that could have appeared to influence the work reported in this paper.

Acknowledgement

The authors would like to thank Professor Zhanfeng Shen from Aerospace Information Research Institute of Chinese Academy of Sciences for data support and valuable suggestions on preparatory work of experiments.

Funding

This research has been jointly supported by the National Key Research and Development Program of China (2018YFC1505501), the National Natural Science Foundation of China (41872253), and the Fundamental Research Funds for the Central Universities.

References

Abdollahi, A., Pradhan, B., Shukla, N., Chakraborty, S., Alamri, A., 2020. Deep Learning Approaches Applied to Remote Sensing Datasets for Road Extraction: A State-Of-The-Art Review. Rem. Sens. 12, 1444.
Chen, Y., Ming, D., Ling, X., Lv, X., Zhou, C., 2021a. Landslide Susceptibility Mapping Using Feature Fusion-Based CPCNN-ML in Lantau Island, Hong Kong. IEEE J. Sel. Top. Appl. Earth Obs. Remote Sens. 14, 3625–3639.
Chen, Y., Weng, Q., Tang, L., Liu, Q., Zhang, X., Bilal, M., 2021b. Automatic mapping of urban green spaces using a geospatial neural network. Gisci. Rem. Sens. 58, 624–642.
Cotrufo, S., Sandu, C., Giulio Tonolo, F., Boccardo, P., 2018. Building damage assessment scale tailored to remote sensing vertical imagery. Eur. J. Rem. Sens. 51, 991–1005.
Dikshit, A., Pradhan, B., Alamri, A.M., 2021. Pathways and challenges of the application of artificial intelligence to geohazards modelling. Gondwana Res. 100, 290–301.
Dong, L., Shan, J., 2013. A comprehensive review of earthquake-induced building damage detection with remote sensing techniques. ISPRS J. Photogramm. Rem. Sens. 84, 85–99.
Dou, A., Wang, X., Ding, X., Yuan, X., Wang, L., Dong, Y., Jin, D., 2012. Quantitative Methods of Rapid Earthquake Damage Assessment Using Remote Sensing and Its Application in Yushu Earthquake. J. Catastrophol. 27, 75–80.
Dubois, D., Lepage, R., 2013. Automated building damage classification for the case of the 2010 Haiti earthquake. In: 2013 IEEE International Geoscience and Remote Sensing Symposium -, pp. 695–698.
Grünthal, G., 1998. European Macroseismic Scale 1998 (EMS-98). European Seismological Committee.
Gupta, R., Hosfelt, R., Sajeev, S., Patel, N., Goodman, B., Doshi, J., Heim, E., Choset, H., Gaston, M., 2019. xBD: A Dataset for Assessing Building Damage from Satellite Imagery, p. arXiv:1911.09296.
Haralick, R.M., Shanmugam, K., Dinstein, I.H., 1973. Textural Features for Image Classification. IEEE Trans. Syst., Man, Cybernet. SMC-3, 610-621.
Kerle, N., 2010. Satellite-based damage mapping following the 2006 Indonesia earthquake—How accurate was it? Int. J. Appl. Earth Obs. Geoinf. 12, 466–476.
Krizhevsky, A., Sutskever, I., Hinton, G.E., 2012. Imagenet classification with deep convolutional neural networks. Adv. Neural Inform. Process. Syst. 25, 1097–1105.
Lv, X., Ming, D., Chen, Y., Wang, M., 2019. Very high resolution remote sensing image classification with SEEDS-CNN and scale effect analysis for superpixel CNN classification. Int. J. Rem. Sens. 40, 506–531.
Mansouri, B., Hamednia, Y., 2015. A Soft Computing Method for Damage Mapping Using VHR Optical Satellite Imagery. IEEE J. Sel. Top. Appl. Earth Obs. Rem. Sens. 8, 4935–4941.

Matin, S.S., Pradhan, B., 2021. Challenges and limitations of earthquake-induced building damage mapping techniques using remote sensing images-A systematic review. Geocarto Int. 1–27.
Monfort, D., Negulescu, C., Belvaux, M., 2019. Remote sensing vs. field survey data in a post-earthquake context: Potentialities and limits of damaged building assessment datasets. Rem. Sens. Appl.: Soc. Environ. 14, 46–59.
Plank, S., 2014. Rapid Damage Assessment by Means of Multi-Temporal SAR — A Comprehensive Review and Outlook to Sentinel-1. Rem. Sens. 6, 4870–4906.
Shao, J., Tang, L., Liu, M., Shao, G., Sun, L., Qiu, Q., 2020. BDD-Net: A General Protocol for Mapping Buildings Damaged by a Wide Range of Disasters Based on Satellite Imagery. Rem. Sens. 12, 1670.
Song, D., Tan, X., Wang, B., Zhang, L., Shan, X., Cui, J., 2020. Integration of super-pixel segmentation and deep-learning methods for evaluating earthquake-damaged buildings using single-phase remote sensing imagery. Int. J. Rem. Sens. 41, 1040–1066.
Syifa, M., Kadavi, P.R., Lee, C.-W., 2019. An Artificial Intelligence Application for Post-Earthquake Damage Mapping in Palu, Central Sulawesi, Indonesia. Sensors 19, 542.
Valentijn, T., Margutti, J., van den Homberg, M., Laaksonen, J., 2020. Multi-Hazard and Spatial Transferability of a CNN for Automated Building Damage Assessment. Rem. Sens. 12, 2839.
Van den Bergh, M., Boix, X., Roig, G., Van Gool, L., 2015. SEEDS: Superpixels Extracted Via Energy-Driven Sampling. Int. J. Comput. Vision 111, 298–314.
Vetrivel, A., Gerke, M., Kerle, N., Nex, F., Vosselman, G., 2018. Disaster damage detection through synergistic use of deep learning and 3D point cloud features derived from very high resolution oblique aerial images, and multiple-kernel-learning. ISPRS J. Photogramm. Rem. Sens. 140, 45–59.
Wang, X., Dou, A., Ding, X., Li, Y., 2015. Advance on the RS-based Emergency Seismic Intensity Assessment. J. Geo-Inform. Sci. 17, 1536–1544.
Weng, Q., 2012. Remote sensing of impervious surfaces in the urban areas: Requirements, methods, and trends. Rem. Sens. Environ. 117, 34–49.
Zheng, Z., Zhong, Y., Wang, J., Ma, A., Zhang, L., 2021. Building damage assessment for rapid disaster response with a deep object-based semantic change detection framework: From natural disasters to man-made disasters. Rem. Sens. Environ. 265, 112636.